Check for updates

One pot synthesis of cyclodextrin MOF as a promising heterogeneous catalyst for the reduction of nitroaromatic compounds and azo dyes

Adnan Shahzaib[1] · Shaily[1] · Iftkhar Ahmad[2] · Fahmina Zafar[1] ·
Saad M. Alshehri[3] · Sajid Ali[4] · Nahid Nishat[1]

Abstract

The fabrication of beta-cyclodextrin with nickel incorporation (Ni–BCD–MOF) for the catalytic reduction of nitroaromatic compounds and dyes has been done using a simple, sustainable, and easy vapor deposition technique. The Ni–BCD–MOF was created using only environmentally safe solvents, promoting sustainable development without adversely affecting the environment. The Fourier transform infrared was utilized for the structural elucidation of prepared Ni–BCD–MOF, and UV–visible spectroscopy divulged a narrow band gap (2.15 eV). The X-ray diffraction pattern depicted the crystallinity of Ni–BCD–MOF. Scanning electron microscopy revealed ingot/brick-type crystal structure with an average particle size of 1.92 μm. The Ni–BCD–MOF exhibited high thermal stability up to 300 °C confirmed via thermogravimetric analysis. Furthermore, BET studies of Ni–BCD–MOF revealed a surface area of 21.1 $m^2 \, g^{-1}$, which is comparatively higher than the surface area of MOFs synthesized with BCD. The Ni–BCD–MOF manifested impeccable performance in reducing nitroaromatics compounds and dyes (≤ 5 min). Ni–BCD–MOF may be used as a suitable substitute for nanocatalysts to reduce organic contaminants due to its high thermal stability, surface area, and catalytic rate constant for reducing azo dyes and nitroaromatic compounds.

✉ Nahid Nishat
   nishat_nchem08@yahoo.com

1   Inorganic Materials Research Lab, Department of Chemistry, Jamia Millia Islamia,
    New Delhi 110025, India

2   Bio/Polymer Research Laboratory, Department of Chemistry, Jamia Millia Islamia University,
    New Delhi 110025, India

3   Department of Chemistry, College of Science, King Saud University, Riyadh, Saudi Arabia

4   Department of Chemistry, Hanyang University, Seoul 133731, South Korea

Graphical abstract
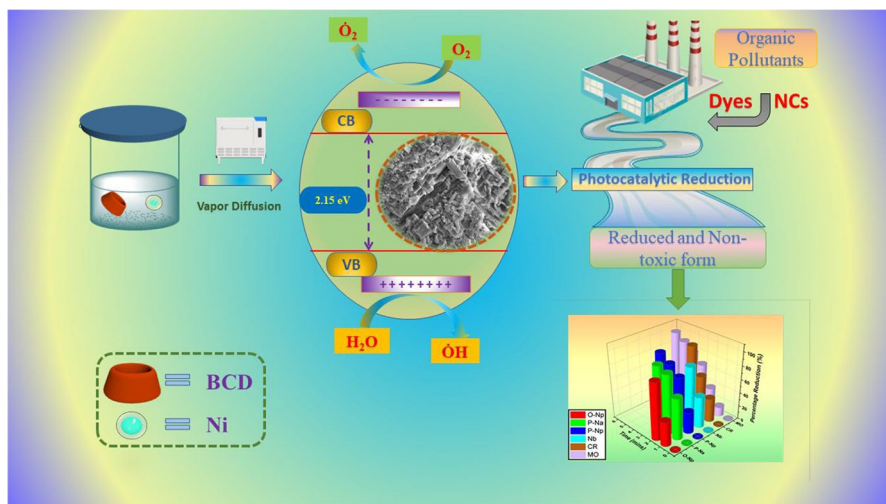
Keywords Cyclodextrin metal–organic frameworks · Catalytic reduction · Nitroaromatics · Dyes · Green Chemistry

Introduction

Metal–organic frameworks (MOFs) are a novel type of porous coordination polymers concocted by the covalent bonding of inorganic nodes and organic ligands and have piqued interest due to their remarkable features [1, 2].Through various synthesizing approaches, a multitude of substances can be modulated in order to adjust their form, size, arrangement, or combination for usage in assorted areas, including gas adsorption [3, 4], energy storage [5, 6], separation [7, 8], biomedicine [9, 10], purification [11, 12], drug delivery systems [13–15], adsorption [16] and catalysis [17–20].

Unfortunately, the overwhelming majority of MOFs produced so far are made up of organic subunits that are hazardous and sourced from non-renewable petrochemical feedstocks that inhibit their applicability in biological and environmental remediation. The challenges of synthesizing them on a relatively large industrial scale include exorbitant costs, disposal concerns, and contamination. Therefore, embracing green principles and implementing them in synthesis, development, and application is becoming the paradigm in the 21st millennium. As a result, the pathways utilized to synthesize MOFs must be from natural sources that are ecologically safe, non-toxic, and based on renewable resources. Bio-MOFs (Biological Metal–Organic Frameworks) refer to MOFs created using natural precursors like nucleobases, porphyrins, and oligosaccharides [21].

Among oligosaccharides, cyclodextrin (CD), a cyclic saccharide, is produced in large quantities by enzyme activity on starch. CDs exist in three forms, α, β, and γ, and their combination with metal form cyclodextrin metal–organic frameworks (CD–MOFs), which are economical and "natural". Stoddart et al. created the first CD–MOF using edible products in 2010 [22]. Since then, numerous CD–MOFs have been created by combining cyclodextrin derivatives with alkali metals, and their applications range from drug administration to adsorption and separation [23].

Nitroaromatics compounds are widely used as a vital chemical raw material in several industries. The intermediate product is an intermediary in producing various products like cosmetics, pharmaceuticals, dyes, and agriculture [24, 25]. Additionally, the industries color their products with carcinogenic dyes like Methyl Orange (MO) and Congo Red (CR). Their uncontrolled flux onto aquatic streams poses an environmental threat. These nitroaromatics compounds are ubiquitous in soil and aqueous habitats; their high concentration adversely affects plant and aquatic organisms [26]. Several physical, chemical, and biological removal and degradation methods, including adsorption [27], electrochemical treatment [28], oxidation, and microbial and photocatalytic reduction, are available to mitigate the toxicity of these nitroaromatics compounds and dyes.

Although these technologies have effectively treated nitroaromatics compounds and dyes at a micro-scale, adequate industrial implementation is still elusive, considering factors such as immense cost and impracticality at a large scale [29]. Among all approaches used for nitroaromatics compounds elimination, photocatalytic reduction utilizing a catalyst to reduce nitroaromatics compounds and dyes is a swift and environmentally benign approach. Many compounds, notably ZnO, TiO_2, and CdS, have been employed as catalysts. However, they have drawbacks like a high band gap and typically entail an outside power source for excitation, which is excessive and time-consuming. Nanoparticles [30], nanocomposites, and MOFs are alternative options for reducing these nitroaromatics compounds. However, owing to their high price, the complex synthesis process hinders their applicability [31]. Takashi et al. synthesized an amino-functionalized MOF exhibiting outstanding catalytic reduction of nitrobenzene [32].

In another study, ZIF-67 was directly pyrolyzed, and nanoparticles were doped, resulting in an amplified reduction of 4-nitrophenol [33]. Gu et al. [34] synthesized Ag/ZIF-8@ZIF-67 MOFs as catalysts for reducing 4-NP. Shen et al. adopted nitroreductase (NTR), an enzyme, to synthesize NTR@ZIF-8, which has high thermal and chemical stability and superior catalytic activity in reducing nitrophenol [35]. Bimetallic MOFs were developed by calcining ruthenium nanoparticles with zinc-based MOFs and were employed in the reduction of nitrophenol and rhodamine dye [36]. However, biobased MOFs are yet to be explored in removing nitroaromatics compounds and dyes.

This work explores the association of simple, toxic-free solvent, and environmentally friendly synthesis of Ni–BCD–MOF at ambient temperature, implementing beta-cyclodextrin (BCD) as the ligand and nickel(II) acetate as the metallic source for reducing nitroaromatics compounds and dyes. The synthesized MOF was evaluated in a variety of ways, including Fourier Transform Infrared Spectroscopy (FTIR), Powder X-ray Diffraction (PXRD), Ultraviolet–visible spectroscopy (UV),

Field Emission Scanning Electron Microscopy (FE-SEM), Elemental Analysis (EDX), and Thermogravimetric Analysis (TGA). Ni–BCD–MOF has been studied as a catalyst for further catalytic reduction of several nitroaromatics compounds, including *p*-nitrophenol (P-Np), Nitrobenzene (Nb), *o*-nitrophenol (O-Np), and *p*-nitroaniline (P-Na), as well coloring dyes like MO and CR.

Experimental

Chemicals

Beta-cyclodextrin (BCD, MW 1135 g/mol) was purchased from SRL. Nickel (II) Acetate (MW 248.84 g/mol) acquired from Qualigens Fine Chemicals, Ethyl alcohol, Methyl alcohol, P-Np (98%), P-Na (99%), Nb (99%), O-Np (98 %), Sodium borohydride (NaBH4 MW 37.8 g/mol), MO (MW 327.3 g/mol) and CR (MW 696.6 g/mol) were bought from Merck.

Fabrication of Ni–BCD–MOF

Ni–BCD–MOF was produced by utilizing the vapor diffusion process and a few minor alterations to the previously recognized strategy for CD–MOF synthesis [22]. In brief, 1.1 g (1 mmol) of BCD was dissolved in 10 mL of water and 2 mL of ethyl alcohol and placed on a magnetic stirrer at room temperature (RT) for 15 min until a clear solution was obtained. In a separate beaker, 1.24 g (5 mmol) of nickel(II) acetate was dissolved and agitated for 10 min at RT in 5 mL of water. The solution was combined and stirred for 5 min to mix both compounds thoroughly. The liquid solution was then transferred to a beaker comprising 60 mL of methyl alcohol and was encased with aluminum foil. The solution was then placed in an oven at 60 °C for 4 days. After that, the solution was removed, and greenish Ni–BCD–MOF crystals were collected and rinsed with ethyl alcohol multiple times to remove impurities before drying in an oven overnight at 80 °C. Figure 1 displays the schematic structure of Ni–BCD–MOF.

Instrumentation

FTIR measurements have been carried out on the Perkin Elmer Spectrophotometer, having a range (of 4000–500 cm^{-1}) and an average of 46 scans at 4 cm^{-1} resolution at RT (28–30 °C). Data collection was performed by utilizing IR solution software. FTIR Spectroscopy (Bruker Optic, Vertex 70 V) was used to evaluate the compounds' functional groups. An X-ray diffractometer (Rigaku Smart Lab Guidance) with Cu Kα radiation was used to assess the MOF's structural composition. The morphological and structural investigation of the material was analyzed (FE-SEM) on an FEI Netherlands, Model No Nova Nanosem-450. Gemini SEM 500 was used for the EDX (Zeiss). A Mettler Toledo device was used to present the findings
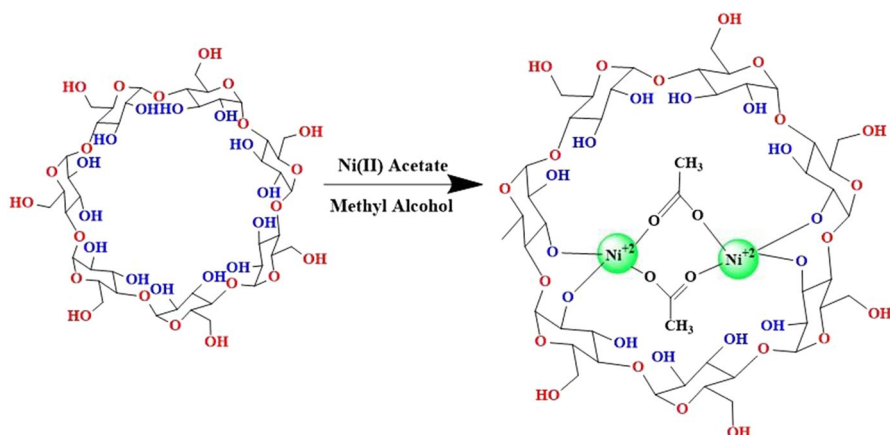
Fig. 1 Schematic structure of Ni–BCD–MOF

of the thermogravimetric investigation (TGA Flow rate 10 °C min⁻¹, Columbus, OH, USA). UV spectroscopy (Shimadzu) was used to assess absorption activity by obtaining absorbance spectra from 200 to 800 nm. The Ni–BCD–MOF surface area and pore size were measured by BET surface area analyzer at 77 K temperature using the Nova 2000e instrument, Quantachrome Instruments Limited. For analysis, about 75 mg of Ni–BCD–MOF was taken in the sample cell and allowed for vacuum degassing for 6 h at 120 °C to remove the moisture and adsorbed gases. The estimation of surface area was done by using a multipoint BET equation. From N_2 desorption isotherms, Dubinin–Astakhov (DA) and Barrett–Joyner–Halenda (BJH) methods were employed to determine the pore size and pore volume distribution.

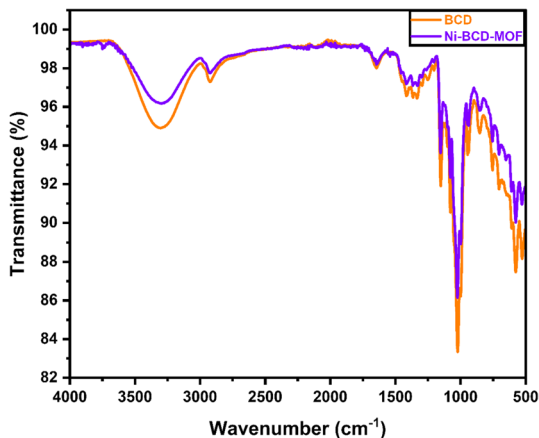## Catalytic reduction of nitroaromatics compounds

To assess the catalytic reduction of nitroaromatics compounds, 1 mL (1 mM) solution of every nitroaromatics compounds viz. P-Np, Nb, O-Np, and P-Na were dispensed into a conventional quartz cuvette. The cuvette was also filled with 1 mL of double-distilled water, 1 mL of $NaBH_4$, and 1 mg of Ni–BCD–MOF catalyst. At RT, UV spectra were analyzed at 60 second intervals.

Catalytic reduction of dyes (MO and CR)

An initial measurement of 100 mg L⁻¹ MO was made in the cuvette. This solution was supplemented with 1 mL each of $NaBH_4$ and H_2O. Then, 1 mg of the synthesized Ni–BCD–MOF was supplemented into this mixture. It was inserted immediately into a UV spectrometer, and the catalytic process was monitored by measuring absorbance every 60 second. For CR reduction, a similar approach was utilized.

The percentage reduction of nitroaromatics compounds/dyes was computed using the following calculation Eq. (1).

$$\text{Percentage Reduction} = \frac{C_i - C_f}{C_i} * 100 \tag{1}$$

C_i and C_f are the initial and final concentrations of nitroaromatics compounds/dyes.

Results and discussion

FTIR

Infrared spectroscopy can be used to estimate cyclodextrin's interaction with the metal ion. Figure 2 depicts the FTIR spectra of BCD and Ni–BCD–MOF. In the spectra of BCD, the peak between 3300 and 3400 cm^{-1} exhibits the symmetrical and asymmetrical vibration of the –OH group, while 2924 cm^{-1} is associated with C–H stretching. Peaks at 1152 cm^{-1} and 1022 cm^{-1} are the result of C–O–C and C stretching. The water atoms in the BCD molecule bend in a way that corresponds to the peak at 1644 cm^{-1} [37, 38]. The Ni–BCD–MOF spectra show the peak for the O–H group at 3317 cm^{-1}, albeit with a lower intensity than BCD. Ni–BCD–MOF contains all the prominent peaks at 2926 cm^{-1}, 1645 cm^{-1}, 1153 cm^{-1}, 1024 cm^{-1}, and 858 cm^{-1}, which correspond to C–H, H–O–H, C–O–C, C–O, and C–C stretching, respectively [39]. These results suggest that the synthesis of Ni–BCD–MOF was successful. Thus, the cyclodextrin structure was retained in Ni–BCD–MOF as evidenced by the comparison of the FTIR spectra of BCD and Ni–BCD–MOF.

Optical analysis

Ni–BCD–MOF UV absorption spectra were measured between 250 and 800 nm, and their spectra are shown in Fig. 3. The absorption peaks at 395 nm correlate with

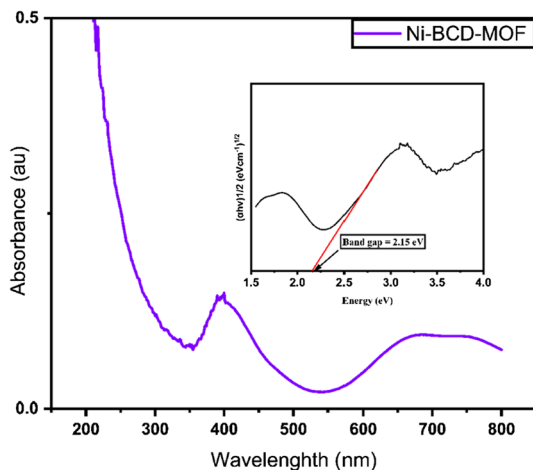**Fig. 3** UV–Vis of Ni–BCD–MOF and inset figure showing band gap value

Table 1 Band gap values of different Ni–BCD–MOF and BCD complexes

S. No.	MOF	Band gap (eV)	References
1	GaO(OH)–CD	5.37	[41]
2	TiO_2/BCD	3.31	[42]
3	ZnO/BCD	3.23	[42]
4	ZnO–BCD	3.17	[43]
5	Ni–MOF-5	3.69	[44]
6	Ni–MOF	3.11	[45]
7	Ni–MOF-74	2.31	[46]
8	Ni–BCD–MOF	2.15	This work

the manifestation of Ni(II) ions [40]. Figure 3 (inset) denotes the band gap energy analyzed via the Tauc equation (2) mentioned as follows:

$$(\alpha h \upsilon)^2 = A\left(h\upsilon - E_g\right) \qquad (2)$$

where α = absorption coefficient, h = Planck's constant, υ = photon's frequency, A = proportionality constant and E_g = band gap energy.

The computed band gap energy is 2.15 eV, higher than other nickel-based-MOF and BCD complexes previously reported, as summarized in Table 1. Owing to its low band gap value, Ni–BCD–MOF may be excited to produce more electron–hole pairs when exposed to light, making it an effective catalyst.

Morphological and elemental studies

The crystallinity of the produced Ni–BCD–MOF was assessed using the PXRD technique and the peak intensities were matched with single crystal PXRD pattern of cyclodextrin MOF (CIF-File no 1041782) [47] to validate the purity of the
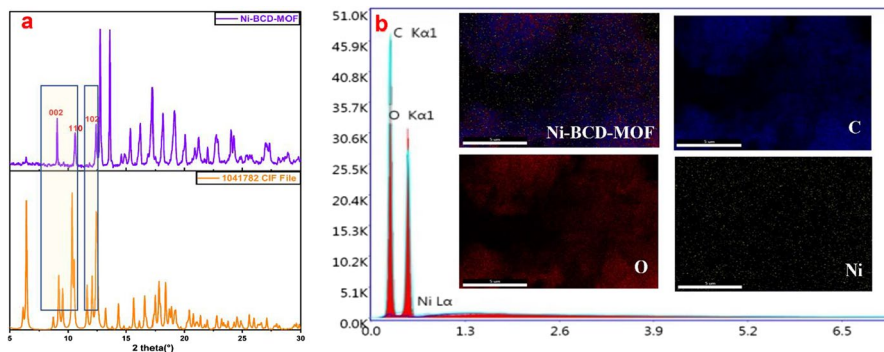
Fig. 4 **a** XRD spectra of Ni–BCD–MOF. **b** Elemental mapping of Ni–BCD–MOF

compound and is shown in Fig. 4a. The results imply that Ni–BCD–MOF was predominantly crystalline, and the diffraction peaks appear at 9.0° (002), 10.7° (110), and 12.6° (102), which accords with the earlier findings and are coherent with other BCD–MOF [48]. The crystallite size of Ni–BCD–MOF has been computed by the Debye–Scherrer equation (3) using X'Pert HighScore Plus V3.0. The Scherrer equation revealed an average crystallite size (*D*) of 27 nm, in accordance with the previous studies [49].

$$D = K\lambda/\beta\cos\theta \tag{3}$$

where *D*, *K*, *λ*, *β*, *θ* are crystallite size (nm), Scherrer constant (0.90), X-ray wavelength (1.54 A°), line broadening at FWHM in radians, and Bragg's angle in degree (°).

The Ni–BCD–MOF was elemental analyzed using EDX, a method for detecting the component elements present in the material. According to the elemental mapping results, as shown in Fig. 4b, Ni–BCD–MOF crystals have constituents of the elements C, O, and Ni.

Morphological patterns of the produced Ni–BCD–MOF particles were corroborated by SEM characterization and are displayed in Fig. 5a–c. The shapes of the Ni–BCD–MOF exhibit a dense accumulation of a long ingot/brick-like structure. In general, synthesized γ-CD-MOF has cubic morphologically shaped crystals, whereas BCD-MOF has an arrangement of cuboidal patterns [50]. The average particle size of Ni–BCD–MOF was calculated using Image J software and was found to be 1.92 μm (Fig. 5d), which agrees with that reported in the literature [51].

Thermal studies

A TGA study was carried out to evaluate the thermal stability of BCD and Ni–BCD–MOF, and their curves are presented in Fig. 6. The initial mass loss of 15% in BCD occurs at a temperature of 115 °C and is prompted by the evaporation of H_2O as shown in the TGA thermogram. The second and third degradations of
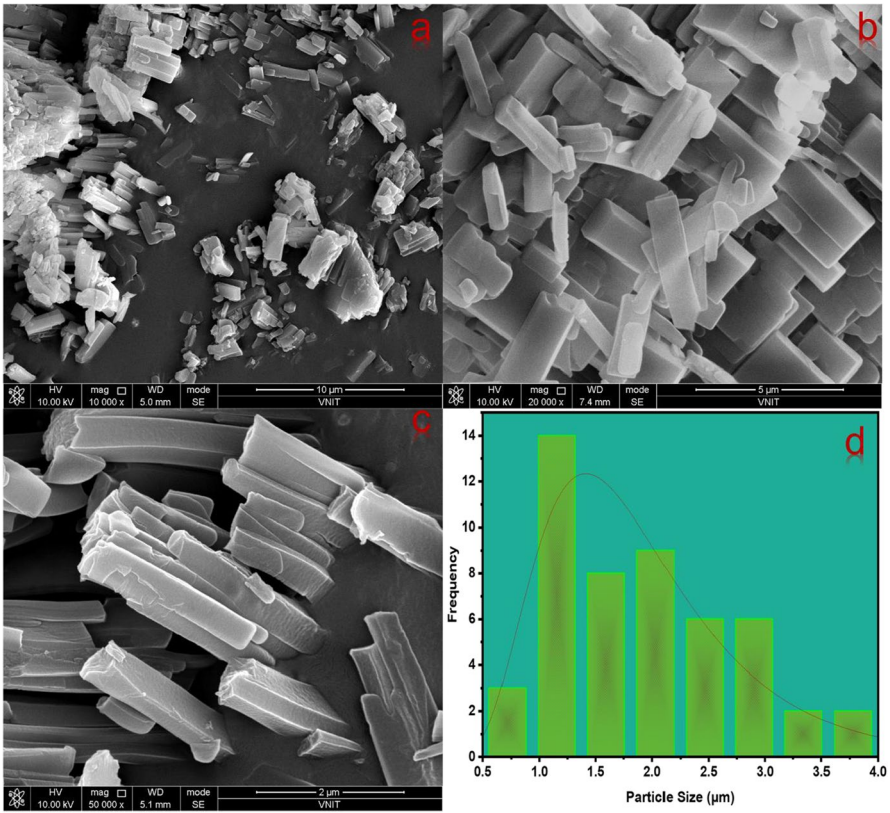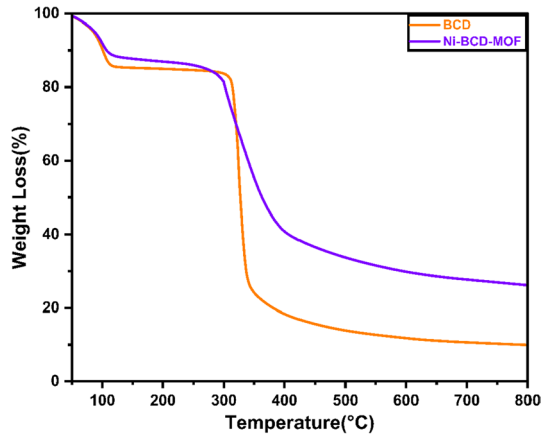
Fig. 5 FESEM image of Ni–BCD–MOF **a** 10 µm, **b** 5 µm, **c** 2 µm, **d** particle size in (µm)

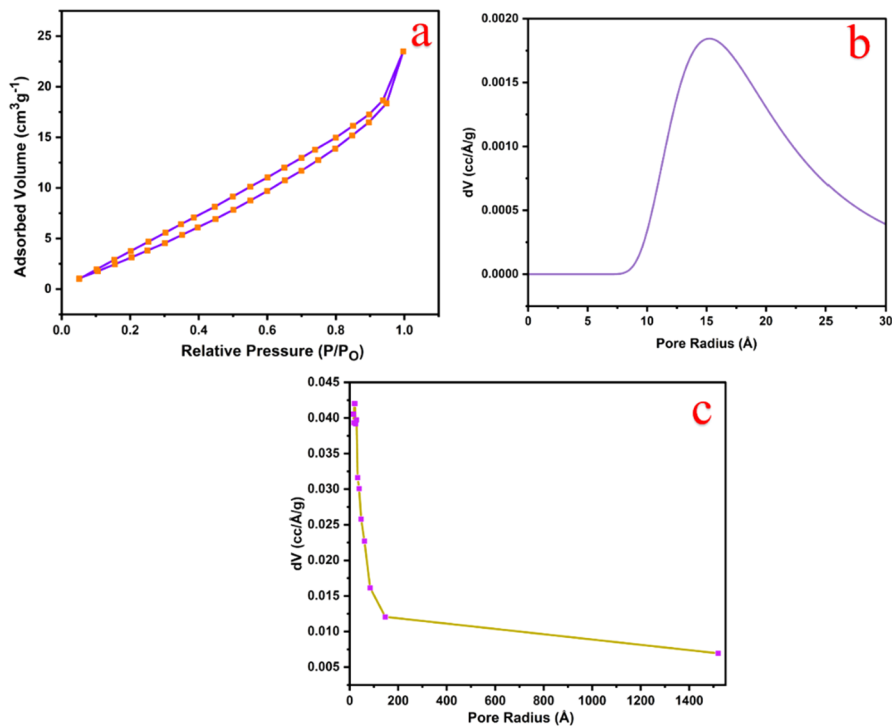**Fig. 6** TGA curve of BCD and Ni–BCD–MOF

Fig. 7 **a** Nitrogen adsorption/desorption isotherm, **b** DA average pore size distribution plot and **c** BJH pore size distribution plot of Ni–BCD–MOF

cyclodextrin are triggered by glucose breakdown at 293 °C and 345–370 °C, respectively, resulting in a loss of 62% mass [52, 53].

Ni–BCD–MOF exhibits higher initial thermal stability than BCD, with the first degradation ranging from 105 to 125 °C with 10% mass loss corresponding to loss of residual solvent molecules and water/methanol. The degradation pattern of Ni–BCD–MOF shows a significant increase in thermal stability compared to cyclodextrin, which can be ascribed to the incorporation of metal ions. The second degradation starts from 275 to 400 °C, amounting to nearly 60% mass loss. BCD–MOFs are typically more thermally stable than other CD–MOFs and thus have the potential to be utilized in applications necessitating thermostability.

BET surface area analysis

BET measurements are a vital tool for the surface area, pore size and pore volume distribution of MOF's surface performances of the materials based on porosity. To analyze the pore size and surface area of the Ni–BCD–MOF sample, N_2 adsorption–desorption evaluations were done using the multipoint BET method. Figure 7a displays the N_2 adsorption–desorption curves of the Ni–BCD–MOF that obeys

the type IV isotherm implying that additional adsorption is occurring. It can be attributed to the strong connection between the adsorbent and the adsorbed layer compared to the connection between the adsorbate and the adsorbent surface that multilayer adsorption is occurring in the adsorbed molecules clustered at higher beneficial sites. Hysteresis of this kind is typically formed through solids comprising agglomerated or aggregated particles that lead to the generation of slit-shaped pores owing to non-uniform shape or size. The surface area of the Ni–BCD–MOF was 21.1 m^2 g^{-1} which was better than reported beta cyclodextrin MOFs [39, 54]. Dubinin–Astakhov (DA) pore size distribution of Ni–BCD–MOF was obtained and found in the range of 11–25 Å, as shown in Fig. 7b. Barrett–Joyner–Helena (BJH) model of average pore size distribution was employed for determining the porosity of Ni–BCD–MOF, as illustrated in Fig. 7c. It infers that the average pore size distribution was in the range of 15–85 Å.

Catalytic studies

Catalytic reduction of nitroaromatics compounds and dyes

Ni–BCD–MOF catalytic capability for reducing nitroaromatics compounds and dyes, namely P-Np, Nb, O-Np, P-Na, MO, and CR was evaluated. Nitroaromatics compounds are frequently employed in industries due to their role in synthesizing pesticides, fertilizers, dye compounds, and medicinal compounds. Nitroaromatics compounds have several negative consequences on marine animals, persons, plants, and other life forms because of their cytotoxic and oncogenic tendency. Reducing them into amino derivatives, which are also applied to fabricate many bioactive molecules, is the ideal way to mitigate their detrimental impacts.

When we exclusively utilize $NaBH_4$, it will take longer for the nitroaromatics compounds and dyes to be converted entirely into a reduced form that is non-toxic without any catalyst. Even after 3 h, appending only $NaBH_4$ leads to a minor reduction of nitroaromatics compounds and dyes, indicating that NaBH4 is not the solitary substance necessary for the reduction, as shown in Fig. 8a–f.

The characteristic peak after adding $NaBH_4$ to the nitroaromatics compounds and dyes, namely P-Np, P-Na, Nb, and O-Np, MO, and CR, is 400, 380, 268, 413, 464, and 494 nm, respectively, shown in Fig. 9a–f. The peak intensity constantly decreases after adding 1 mg of Ni–BCD–MOF catalyst. This dip in peak intensity signifies a drastic reduction in NC levels. When P-Np is present, the peak at 400 nm loses intensity with time, and a gradual rise of peak attributable to 4-aminophenol appears at 303 nm. In the case of P-Na, the band at 380 nm diminishes, and two peaks indicate the formation of 4-aminoaniline at 240 and 306 nm. Similarly, in the case of Nb, the peak at 269 nm wanes, and a peak at 229 nm arises, signifying the emergence of aniline. The peak intensity at 413 nm for the catalytic reduction of O-Np begins to wane as the reaction proceeds, and the formation of peaks at 287–292 nm is associated with the development of 2-aminophenol. The catalytic reduction of nitroaromatics compounds was found to be P-Np (4 min), P-Na (3 min), Nb (2 min), and O-Np (2 min), respectively.
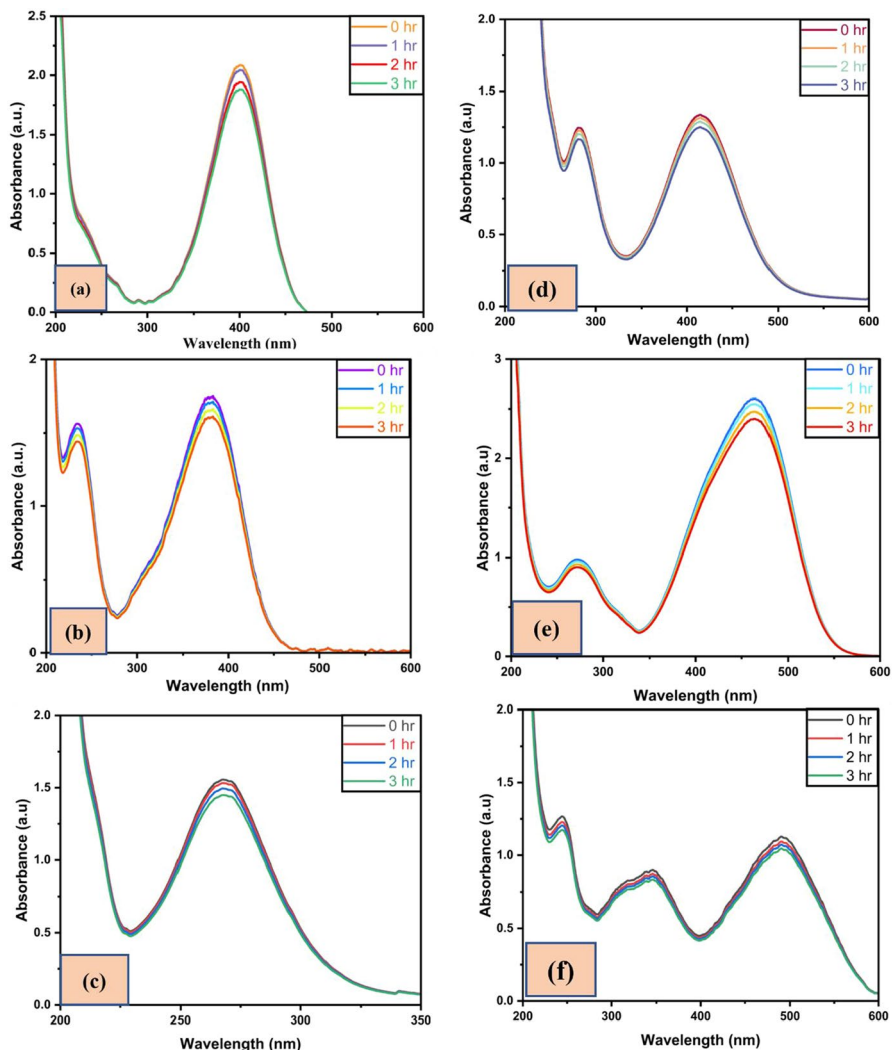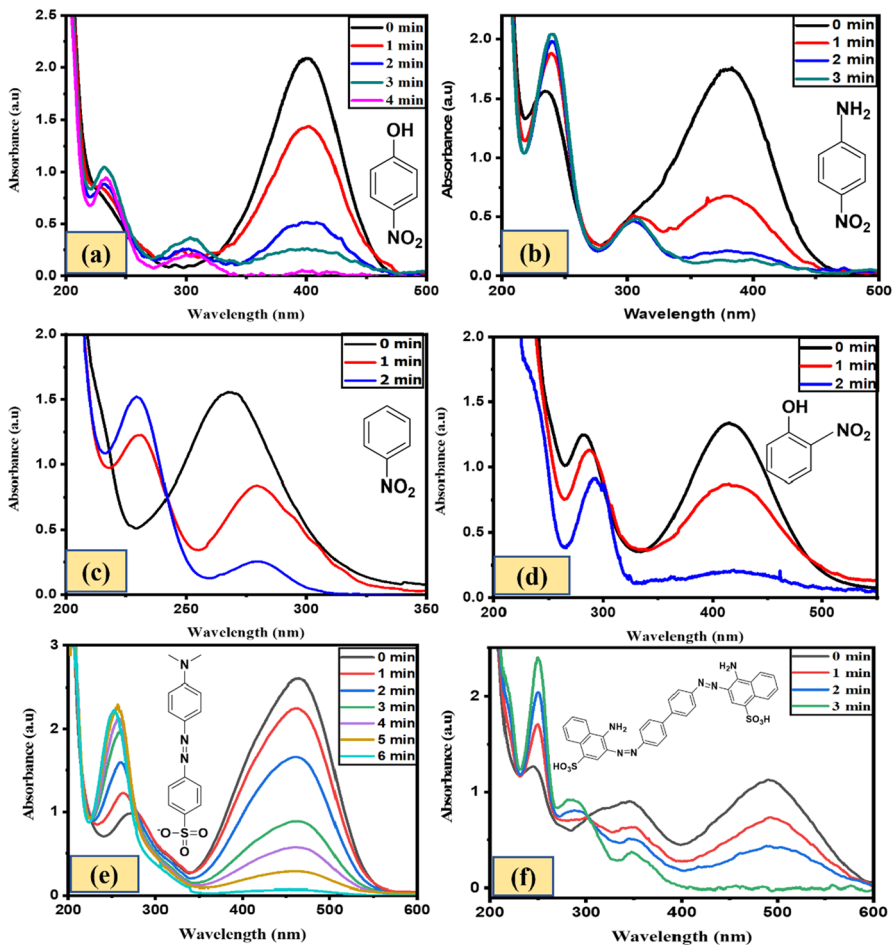
Fig. 8 UV–visible spectra for the reduction of **a** P-Np, **b** P-Na, **c** Nb, and **d** O-Np **e** MO and **f** CR in the presence of NaBH$_4$

A similar approach to the one described previously was used to analyze Ni–BCD–MOF's effectiveness at reducing dyes. The UV absorption peak of MO is typically at 464 nm, with a secondary peak at 274 nm, as seen in Fig. 9e. The peak intensity at 464 nm decreases significantly with the inclusion of the catalyst. The peak at 274 nm is blue-shifted, with an intensity reaching 257 nm indicating MO reduction.

There are two prominent absorption spectra in the UV region of the CR spectrum, at 494 and 346 nm, respectively. When a catalyst is not involved, there is no variation in the peak intensity. However, when Ni–BCD–MOF gets involved, there

Fig. 9 UV–visible spectra for the reduction of **a** P-Np, **b** P-Na, **c** Nb, **d** O-Np, **e** MO, and **f** CR using Ni–BCD–MOF in the presence of NaBH$_4$

is a significant reduction in the peak intensity at 494 and 346 nm, which can be seen in Fig. 9f. The simultaneous peak emergence indicated the reduction process at 250 nm, which occurred concurrently with the reduction in peak intensity.

Given that the concentration of nitroaromatics compounds is negligible compared to that of NaBH$_4$, pseudo-first-order rate kinetics was used to examine the rate constant. The rate constant was calculated using the following equation (4):

$$\ln \frac{C_t}{C_o} = \ln \frac{A_t}{A_o} = -k_{app}t \tag{4}$$

where C_t/C_o is the ratio of the nitroaromatics compounds concentration at time t to the lambda maximum (λ_{max}) at time $t = 0$, the k_{app} values are assessed from the linear fitting of ln C_t/C_o verses time plots and are displayed in Fig. 10a–f. The catalyst
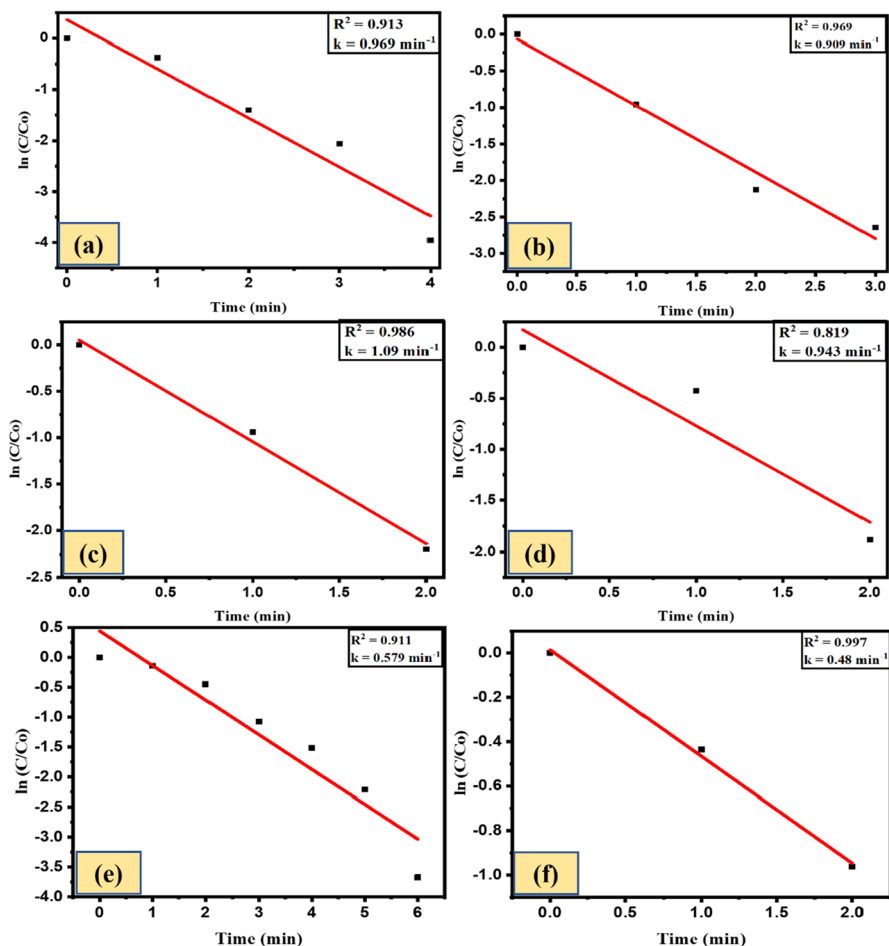
Fig. 10 Plot of ln C/C_o verses time for **a** P-Np, **b** P-Na, **c** Nb, **d** O-Np, **e** MO, and **f** CR using Ni–BCD–MOF in the presence of $NaBH_4$

is observed to convert nitroaromatics compounds and dyes to their derivatives, with rate constants of 0.96, 0.90, 1.09, 0.94, 0.57, and 0.48 min^{-1} for P-Np, P-Na, Nb, O-Np, MO, and CR, respectively. These findings signify that Ni–BCD–MOF seems to have an excellent catalytic efficiency for reducing dyes and nitroaromatics compounds.

The nitroaromatics compounds, dye catalytic rate constants and associated regression coefficients (R^2) are listed in Table 2. The percentage reduction of nitroaromatics compounds from the corresponding UV spectrums was calculated using Eq. (1). The reduction of P-Np, P-Na, Nb, O-Np, CR, and MO to their corresponding derivatives rapidly takes 4, 3, 2, 2, 3, and 6 min, respectively. The observed percentage reductions for P-Np, P-Na, Nb, O-Np, CR, and MO are 97.27%, 92.98%, 83.45%, 84.67%, 99.82%, and 97.46%, respectively.

Table 2 Catalytic reduction of different nitroaromatics compounds and dyes

Organic pollutants	Rate constant (min^{-1})	Time (min)	R^2	Percentage reduction
P-Np	0.969	4	0.913	97.27
P-Na	0.909	3	0.969	92.98
Nb	1.09	2	0.986	83.45
O-Np	0.943	2	0.819	84.67
CR	0.48	3	0.997	99.82
MO	0.579	6	0.911	97.46
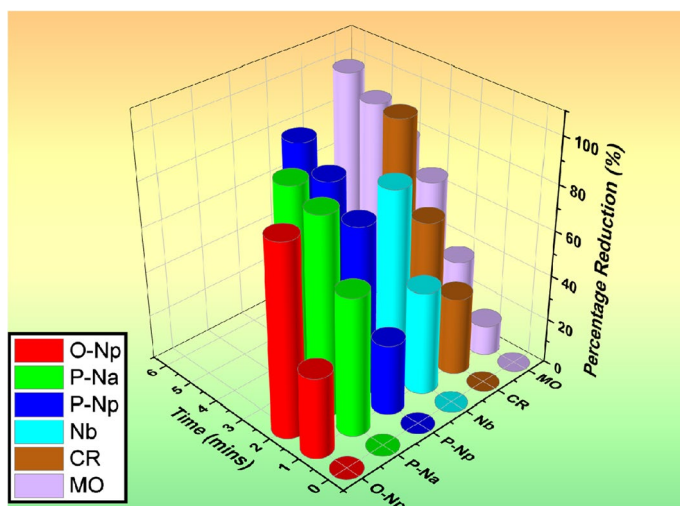
Fig. 11 Percentage reduction with the time of nitroaromatics compounds and organic dyes via Ni–BCD–MOF

The percentage reduction with the time graph for nitroaromatics compounds and dyes is presented in Fig. 11. Different organic pollutants (nitroaromatics compounds and dyes) and their product formation with λ_{max} values are provided in Tables 3 and 4.

Mechanism

Based on the literature, a plausible mechanism for reducing nitroaromatics compounds is given in Fig. 12. The catalytic reduction of organic pollutants is assumed to follow the Langmuir–Hinshelwood model. We use the case of P-Np in order to comprehend the mechanism better. When P-Np molecules are contacted with BH_4^- ions, they undergo a transformation that results in 4-nitrophenolate ions. The BH_4^- ions produced would donate electrons to the Ni–BCD–MOF, and the reduction of water would result in the formation of active hydrogen atoms,

Table 3 Structure of selected nitroaromatics compounds and their possible product formed after the reduction with the synthesized Ni–BCD–MOF
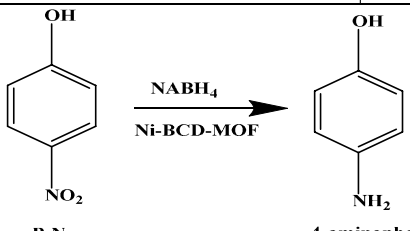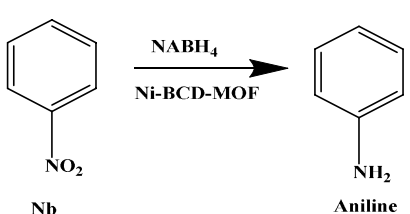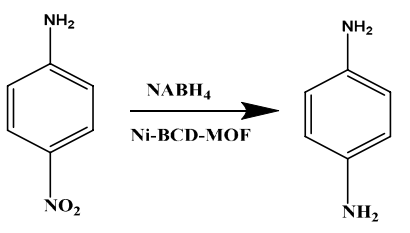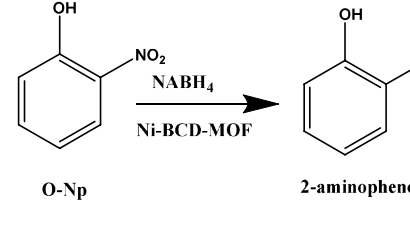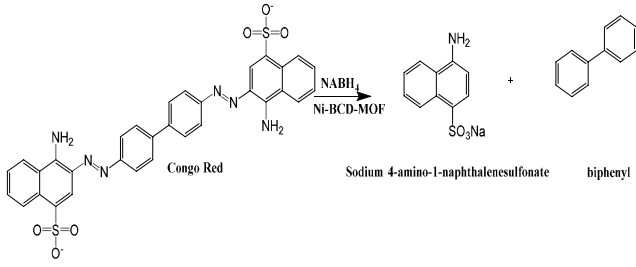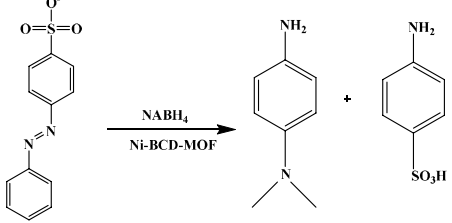
Organic Pollutant		Product	λmax (nm) after the addition of NaBH$_4$	λmax (nm) of final product formed
OH — NO$_2$ — P-Np	NABH$_4$ / Ni-BCD-MOF	OH — NH$_2$ — 4-aminophenol	400	228 and 297
NO$_2$ — Nb	NABH$_4$ / Ni-BCD-MOF	NH$_2$ — Aniline	268	230
NH$_2$ — NO$_2$ — P-Na	NABH$_4$ / Ni-BCD-MOF	NH$_2$ — NH$_2$ — 4-aminoaniline	380	238 and 305
OH — NO$_2$ — O-Np	NABH$_4$ / Ni-BCD-MOF	OH — NH$_2$ — 2-aminophenol	413	286

Table 4 Structure of dyes and their possible product formed after the reduction with the synthesized Ni–BCD–MOF

Organic Pollutant	Product	λmax (nm) after the addition of NaBH₄	λmax (nm) of final product formed
Congo Red	Sodium 4-amino-1-naphthalenesulfonate + biphenyl	494	250
Methyl Orange	N-N dimethyl-benzene-1,4 diamine + 4-amino-benzene sulfonic acid	464	257

which get adsorbed on the surface of the Ni–BCD–MOF. In the subsequent phase, 4-nitrophenolate ions are immobilized on the catalyst and transformed into 4-hydroxylaminophenol. P-Np units can be quickly adsorbed on the surface of Ni–BCD–MOF because of their π–π stacking interaction and large surface area, which promotes the interactions of P-Np and Ni–BCD–MOF. Now, 4-AP is formed due to the reduction of 4-hydroxylaminophenol. Finally, the final product is desorbed from the catalyst's surface, which may be reused in the subsequent catalytic cycle.

In the case of azo dyes (CR), the surface of Ni–BCD–MOF is decorated with BH_4^- ions generated via the dissociation of NaBH₄ and CR molecules in an aqueous solution. BH_4^- ions serve as a hydrogen source. After an electron transfer from BH_4^- ions to Ni–BCD–MOF, hydrogen is liberated and attacks CR dye molecules. The oxygen and sulfur atoms of CR molecules bind to the surface of Ni–BCD–MOF. Conjugation weakens their azo double bonds, resulting in their dissociation. Upon
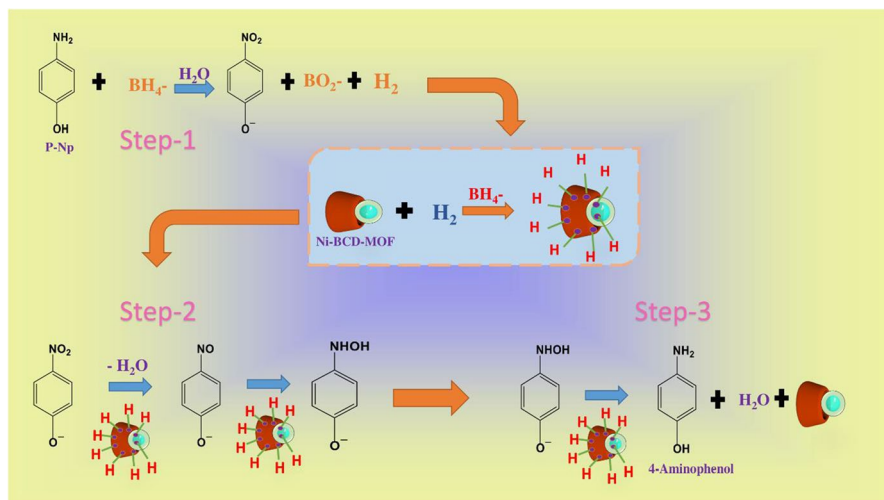
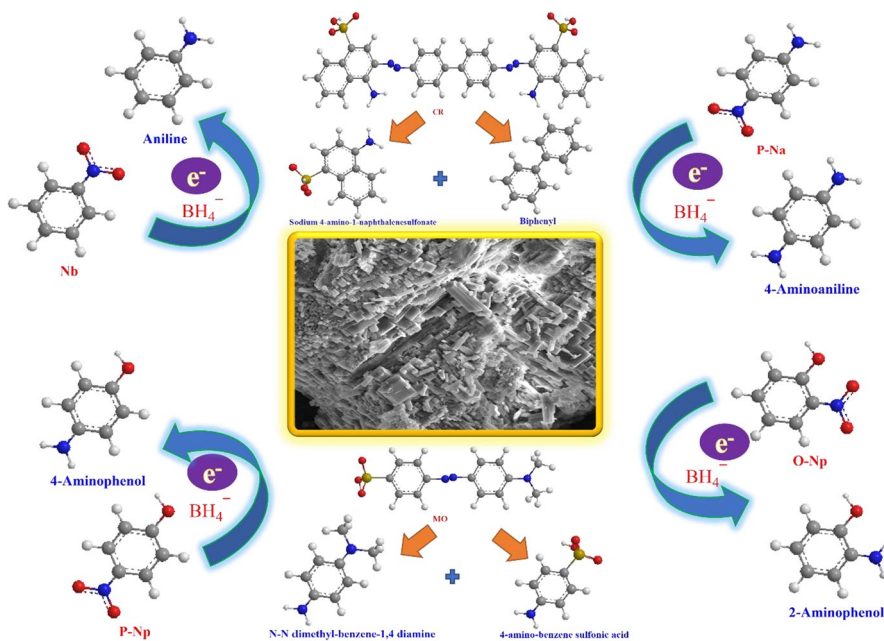**Fig. 12** Plausible mechanism for reduction of P-Np by NaBH$_4$ by Ni–BCD–MOF

Fig. 13 Catalytic reduction of nitroaromatics compounds and organic dyes to their derivatives by Ni–BCD–MOF

Table 5 Comparison of other reported catalysts with synthesized Ni–BCD–MOF

Catalyst	Pollutant	Rate constant (min^{-1})	Time (min)	References
Cu–Ag/GP	P-Np	0.243	10	[55]
	O-Np	0.0726	16	
	MO	0.4602	4	
	CR	0.1338	7	
Cu–Ni/GP	P-Np	0.3648	7	
	O-Np	0.0666	19	
	MO	0.2376	5	
	CR	0.228	6	
Ni–Ag/GP	MO	0.1032	10	
Cu/Cu$_2$O	P-Np	NM	10	[56]
Fe$_3$O$_4$/Ni	P-Na	NM	12	[57]
Cu NPs/MPs	CR	0.610	7	[58]
SPION@LT-Cu^0	P-Na	0.381	10	[59]
	P-Np	0.277	10	
	Nb	0.213	9	
	CR	0.20	7	
	MB	0.175	14	
	MO	0.324	10	
Ni–BCD–MOF	P-Np	0.969	4	Present work
	P-Na	0.909	3	
	Nb	1.09	2	
	O-Np	0.943	2	
	CR	0.48	3	
	MO	0.579	6	

NM not mention

completion of the reduction reaction, the CR is colorless due to the initial conversion of the –N=N– bond into the –HN–NH– bond.

Additionally, the catalyst absorbs the hydrogen atoms released by reducing agents, which converts organic contaminants into their subsequent non-toxic state in conjunction with the emitted electron. These reduced substances displayed in Fig. 13 are degradable, less noxious, and non-polluting and thus can be employed as intermediates in the production of a variety of medicinal compounds.

The comparative analyses of other reported catalysts with our synthesized Ni–BCD–MOF are summarized in Table 5.

Conclusion

This study combined transition metal (Ni) with β-CD to generate Ni–BCD–MOF via a facile, toxic-free solvent green approach. Morphological scans indicated a dense cluster of rod-like formations with a high degree of crystalline character. EDX and FTIR analysis confirm successful metal encapsulation with β-CD with an average particle size of 1.92 μm. Furthermore, the catalytic activity of nitroaromatics compounds and dyes was investigated utilizing Ni–BCD–MOF as a catalyst. The results indicated outstanding catalytic reduction for both nitroaromatics compounds and dyes in a relatively short amount of time, equating to a small band gap (2.15 eV), and can be considered a suitable alternative for other semiconductor catalysts like TiO_2 and ZnO. Ni–BCD–MOF can be used as a catalyst to eliminate toxic compounds and be suitable for water treatment.

Declarations

Conflict of interest The authors declare no competing interests.

References

1. V. Safari Fard, Y. Davoudabadi Farahani, J. Appl. Organomet. Chem. **2**, 180 (2022)
2. A. Amiri, F. Ghaemi, B. Maleki, Microchim. Acta **186**, 131 (2019)
3. Z. Cao, L. Chen, S. Li, M. Yu, Z. Li, K. Zhou, C. Liu, F. Jiang, M. Hong, Chem. An Asian J. **14**, 3597 (2019)
4. D. Wu, J. Liu, J. Jin, J. Cheng, M. Wang, G. Yang, Y.-Y. Wang, Cryst. Growth Des. **19**, 6774 (2019)
5. X. Zhang, A. Chen, M. Zhong, Z. Zhang, X. Zhang, Z. Zhou, X.-H. Bu, Electrochem. Energy Rev. **2**, 29 (2019)
6. J. Ren, Y. Huang, H. Zhu, B. Zhang, H. Zhu, S. Shen, G. Tan, F. Wu, H. He, S. Lan, X. Xia, Q. Liu, Carbon Energy **2**, 176 (2020)
7. K.J. Hartlieb, J.M. Holcroft, P.Z. Moghadam, N.A. Vermeulen, M.M. Algaradah, M.S. Nassar, Y.Y. Botros, R.Q. Snurr, J.F. Stoddart, J. Am. Chem. Soc. **138**, 2292 (2016)
8. H. Bux, C. Chmelik, R. Krishna, J. Caro, J. Membr. Sci. **369**, 284 (2011)
9. A. Bieniek, A.P. Terzyk, M. Wiśniewski, K. Roszek, P. Kowalczyk, L. Sarkisov, S. Keskin, K. Kaneko, Prog. Mater. Sci. **117**, 100743 (2021)
10. X. Liu, T. Liang, R. Zhang, Q. Ding, S. Wu, C. Li, Y. Lin, Y. Ye, Z. Zhong, M. Zhou, ACS Appl. Mater. Interfaces **13**, 9643 (2021)

11. B.-M. Jun, Y.A.J. Al-Hamadani, A. Son, C.M. Park, M. Jang, A. Jang, N.C. Kim, Y. Yoon, Sep. Purif. Technol. **247**, 116947 (2020)
12. M. Fu, X. Deng, S.-Q. Wang, F. Yang, L.-C. Lin, M.J. Zaworotko, Y. Dong, Sep. Purif. Technol. **288**, 120620 (2022)
13. D. De, P. Sahoo, Dalton Trans. **51**, 9950 (2022)
14. J. Schnabel, R. Ettlinger, H. Bunzen, ChemNanoMat **6**, 1229 (2020)
15. S. Zirak Hassan Kiadeh, A. Ghaee, M. Farokhi, J. Nourmohammadi, A. Bahi, F.K. Ko, Int. J. Biol. Macromol. **173**, 351 (2021)
16. H. Shayegan, V. Safari Fard, H. Taherkhani, M.A. Rezvani, J. Appl. Organomet. Chem **2**, 109 (2022)
17. A. Shahzaib, Shaily, I.Ahmad, P. Singh, F. Zafar, Y. Akhtar, A.A. Bukhari, N. Nishat, Catal. Commun. **174**, 106569 (2023)
18. R. Taghavi, S. Rostamnia, Chem. Methodol. **6**, 629 (2022)
19. R. Taghavi, S. Rostamnia, Chem. Methodol. **6**, 639 (2022)
20. R. Tayebee, M.F. Abdizadeh, N. Erfaninia, A. Amiri, M. Baghayeri, R.M. Kakhki, B. Maleki, E. Esmaili, Appl. Organomet. Chem. **33**, e4959 (2019)
21. H. Cai, Y.-L. Huang, D. Li, Coord. Chem. Rev. **378**, 207 (2019)
22. R.A. Smaldone, R.S. Forgan, H. Furukawa, J.J. Gassensmith, A.M.Z. Slawin, O.M. Yaghi, J.F. Stoddart, Angew. Chem. Int. Ed. **49**, 8630 (2010)
23. Y. He, X. Hou, Y. Liu, N. Feng, J. Mater. Chem. B **7**, 5602 (2019)
24. C. Wang, H. Zhang, C. Feng, S. Gao, N. Shang, Z. Wang, Catal. Commun. **72**, 29 (2015)
25. M. Bilal, A.R. Bagheri, P. Bhatt, S. Chen, J. Environ. Manag. **291**, 112685 (2021)
26. M. Capodici, A. Avona, V.A. Laudicina, G. Viviani, Sci. Total Environ. **630**, 462 (2018)
27. Laxmi, A. Shahzaib, M. Alam, A. Ghosal, F. Zafar, N. Nishat, J. Appl. Polym. Sci. **139** e52993 (2022)
28. L.-Z. Huang, H.C.B. Hansen, M.J. Bjerrum, J. Hazard. Mater. **306**, 175 (2016)
29. J. Tiwari, P. Tarale, S. Sivanesan, A. Bafana, Environ. Sci. Pollut. Res. **26**, 28650 (2019)
30. H. Veisi, B. Karmakar, T. Tamoradi, R. Tayebee, S. Sajjadifar, S. Lotfi, B. Maleki, S. Hemmati, Sci. Rep. **11**, 4515 (2021)
31. I. Ahmad, G. Aalam, M. Amir, A. Chakravarty, S.W. Ali, S. Ikram, Sci. Total Environ. **846**, 157154 (2022)
32. T. Toyao, M. Saito, Y. Horiuchi, K. Mochizuki, M. Iwata, H. Higashimura, M. Matsuoka, Catal. Sci. Technol. **3**, 2092 (2013)
33. W. Du, F. Han, M. Zhang, C. Qian, X. Yang, Compos. Commun. **25**, 100718 (2021)
34. A. Gu, J. Chen, Q. Gao, M.M. Khan, P. Wang, Y. Jiao, Z. Zhang, Y. Liu, Y. Yang, Appl. Surf. Sci. **516**, 146160 (2020)
35. B. Shen, R. Ding, J. Dai, Y. Ji, Q. Wang, Y. Wang, H. Huang, X. Zhang, Green Synth. Catal. **2**, 367 (2021)
36. W. Liu, W. Duan, Q. Zhang, X. Gong, J. Tian, New J. Chem. **46**, 17004 (2022)
37. R.L. Abarca, F.J. Rodríguez, A. Guarda, M.J. Galotto, J.E. Bruna, Food Chem. **196**, 968 (2016)
38. H. Rachmawati, C.A. Edityaningrum, R. Mauludin, AAPS PharmSciTech **14**, 1303 (2013)
39. T. Volkova, A. Surov, I. Terekhova, J. Mater. Sci. **55**, 13193 (2020)
40. K.S. Anuratha, M. Ramaprakash, S.K. Panda, S. Mohan, Ceram. Int. **43**, 10174 (2017)
41. B.N. Ganguly, V. Verma, D. Chatterjee, B. Satpati, S. Debnath, P. Saha, ACS Appl. Mater. Interfaces **8**, 17127 (2016)
42. S. Rajalakshmi, S. Pitchaimuthu, N. Kannan, P. Velusamy, Appl. Water Sci. **7**, 115 (2017)
43. R. Yadav, T.S. Chundawat, P. Rawat, G.K. Rao, D. Vaya, Bull. Mater. Sci. **44**, 250 (2021)
44. A. Katoch, R. Bhardwaj, N. Goyal, S. Gautam, Vacuum **158**, 249 (2018)
45. X. Ding, H. Liu, J. Chen, M. Wen, G. Li, T. An, H. Zhao, Nanoscale **12**, 9462 (2020)
46. T. Li, Z. Jin, J. Colloid Interface Sci. **605**, 385 (2022)
47. J.-Q. Sha, L.-H. Wu, S.-X. Li, X.-N. Yang, Y. Zhang, Q.-N. Zhang, P.-P. Zhu, J. Mol. Struct. **1101**, 14 (2015)
48. S. Wang, G. Shao, H. Zhao, L. Yang, L. Zhu, H. Liu, B. Cui, D. Zhu, J. Li, Y. He, J. Mater. Sci. **56**, 3049 (2021)
49. J. Suárez-Cerda, H. Espinoza-Gómez, G. Alonso-Núñez, I.A. Rivero, Y. Gochi-Ponce, L.Z. Flores-López, J. Saudi Chem. Soc. **21**, 341 (2017)
50. Z. Hu, S. Li, S. Wang, B. Zhang, Q. Huang, Food Chem. **338**, 127839 (2021)
51. Y. Li, H. Huang, C. Ding, X. Zhou, H. Li, Mater. Lett. **300**, 129766 (2021)

52. I. Shown, S. Banerjee, A.V. Ramchandran, K.E. Geckeler, C.N. Murthy, Macromol. Symp. **287**, 51 (2010)
53. N.K. Vishwakarma, V.K. Patel, S.K. Hira, K. Ramesh, P. Srivastava, K. Mitra, S. Singh, D. Chattopadhyay, P. Maiti, N. Misra, P.P. Manna, B. Ray, RSC Adv. **5**, 15547 (2015)
54. C. Liu, P. Wang, X. Liu, X. Yi, Z. Zhou, D. Liu, A.C.S. Sustain, Chem. Eng. **7**, 14479 (2019)
55. M. Ismail, M.I. Khan, S.B. Khan, M.A. Khan, K. Akhtar, A.M. Asiri, J. Mol. Liq. **260**, 78 (2018)
56. Y. Yu, H. Guo, P. Wang, S. Zhai, J. Han, W. Li, Y. Wang, Y. Wang, Res. Chem. Intermed. **49**, 381 (2023)
57. P.S. Rathore, R. Patidar, T. Shripathi, S. Thakore, Catal. Sci. Technol. **5**, 286 (2015)
58. B.K. Ghosh, S. Hazra, B. Naik, N.N. Ghosh, Powder Technol. **269**, 371 (2015)
59. I. Ahmad, K. Manzoor, G. Aalam, M. Amir, S.W. Ali, S. Ikram, Catal. Lett. https://doi.org/10.1007/s10562-022-04182-1 (2022)